

Microcrystalline Graphite Oxide as Durable Catalyst Support for PEM Fuel Cell

Tu Wenmao*, Pan Qun, Li Yanyan, Wang Nan

School of Resources and Environmental Engineering, Wuhan University of Technology, Hubei Key Laboratory of Mineral Resources Processing and Environment, Wuhan 430070, China

*E-mail: wenmaotu@sina.com

Received: 8 August 2012 / Accepted: 8 October 2012 / Published: 1 November 2012

Microcrystalline graphite oxides are prepared for developing highly durable Pt/C catalyst for fuel cells. Highly dispersed Pt nanoparticles with size about 3.5 nm are deposited on microcrystalline graphite oxide because of the highly functionalized surface. Cyclic voltammetric results demonstrate that the initial activity surface area of Pt/MGO catalyst is 29.0 m²/g_{pt}, much higher than Pt/C catalyst with carbon black as the support (11.7 m²/g_{pt}) because of the surface activity of microcrystalline graphite oxide. The Pt/MGO catalyst also presents durability much better than conventional Pt/C catalyst under acidic electrochemical conditions because of the innate stability of graphite structure. After 1000 CV cycles, the EAS loss of the Pt/MGO catalyst is 2.07 %, extensively lower than those of the Pt/CB catalyst and Pt/GC catalyst.

Keywords: Microcrystalline graphite oxide, catalyst support, PEM fuel cell, durability

1. INTRODUCTION

Proton-exchange membrane fuel cells (PEMFCs) are attractive low-emission power sources for electrically powered vehicles and distributed power generation. The corrosion of catalyst support continues to present challenge for fuel cells to meet the required lifetime. This is especially the case when the fuel cell is operated in transportation applications with extreme or cyclic changes in load [1, 2]. The integrity of the catalyst support is one of the most crucial factors affecting the lifetime of fuel cells because it functions both anchor of the catalyst and electron conductor of the electrochemical reaction. The commonly employed carbon black supports suffer oxidation to surface oxides, and eventually to CO₂ at the cathode during long-term operations in oxygen-rich environment, high operating-potentials and low pH[3-8]. It is also possible for the cathode to attain high potentials for

short periods of time during start-up and shut-down. In practice, repeated start-up/shut-down cycles can lead to short-term potential excursions of the cathode to 1.2–1.5 V causing accelerated carbon corrosion [9-11].

In the past several years, much effort has been geared toward the development of alternative, chemically stable catalyst support for PEM fuel cells. It was reported that durability of the carbon black supports subjected to potential cycling between 0.6 and 0.9 V could be improved by covering with inorganic oxide such as silica[12]. However, the coverage of the whole surface of the catalysts with silica layers produced electrochemically inactive Pt catalysts. Conductive ceramics, such as WC, TiB₂ are also potential catalyst supports for fuel cell with high durability[13]. Zhu et al. synthesized Nano-crystalline WC with surface area of 89 m²/g and found that this type of support had slightly lower electrochemical stability at high surface area condition. Uniformly distributed Pt particle on the WC supports because of low activity of the support was also found to be a concern[14].

Graphitic carbons were considered as promising catalyst supports with high stability in comparison with carbon black. In an acceleration fuel cell test regarding amorphous carbon and graphitized carbon, researchers found that performance degradation of fuel cells with graphitized carbon support were only about 10% in relation to 77% for the one with amorphous carbon support[15]. Catalyst-support interaction is of importance for balancing the stability and performance of the catalyst and support[16]. The shortage of the graphitic carbons was the inert surface with only very limited amount of surface defects for the anchorage of Pt catalyst nanoparticles. Thus, modification of the graphitic carbons surface is necessary to meet the fuel cell performance requirement. A recent research demonstrated N-doped carbon nanotube supports with open ends had both high activity and good resistance to carbon corrosion[17]. Functionalizing carbon nanofibers with pyrenecarboxylic acid also improved the surface activities of the support for Pt catalyst deposition, but sustained the corrosion resistance of carbon nanofibers because it preserves the intrinsic properties of graphitic carbon without damaging their surface structure[18]. Another approach was modifying graphitic carbon fiber with nitrogen doping by pyrolysis of a polyaniline precursor[19]. It was found that the modified graphitic carbons had 5 times lower carbon corrosion compared to carbon based catalyst when potential reached 1.5 V versus RHE in simulated start/stop cycling.

Among the various forms of carbonaceous materials, microcrystalline graphite oxide (MGO) has emerged as a potential catalyst support for fuel cells because of the stability similar to graphite and activity similar to carbon black. Graphite oxide is typically prepared by oxidation of graphite with strong oxidation agents, resulting in the formation of various oxygen groups on the surface and the edges of the graphite layers [20, 21]. In the present work, we synthesized Pt/MGO catalyst and investigated the performance and stability in comparison to graphite and active carbon black. The results demonstrate that the electrochemical activity of the Pt/MGO catalyst is no lower or better than that of Pt/C catalyst with carbon black as the support because of the surface activity of microcrystalline graphite oxide. The Pt/MGO catalyst also presented durability much better than conventional Pt/C catalyst under acidic electrochemical conditions because of the innate stability of graphite structure.

2. EXPERIMENTAL

2.1 Preparation of Pt/C catalyst with carbon black, graphite and microcrystalline graphite oxide as the supports

Microcrystalline graphite oxide (MGO) was synthesized by advanced Hummers method with microcrystalline graphite (Lutang, China) as the raw material. During the preparation, 5 g microcrystalline graphite, 2.5 g of NaNO₃ and 15 g potassium permanganate were added into 115 mL of H₂SO₄ (CR, 98%) and stirred for 1 hours at 0 °C with low temperature thermostatic bath. Then the mixed solution was warmed up to 35±3 °C. After stirring for 30 minutes, the temperature of the solution was further heated to 98±3 °C and stirred for another 15 minutes. After cooling to room temperature, appropriate amount H₂O₂ (5%) was added into the mixed solution to remove the residual potassium permanganate. The as-resulted microcrystalline graphite oxide was obtained with filtering, extensively washing by DI water, and vacuum drying at 50 °C for 24 hours.

The Pt electrocatalyst supported on active carbon black (XC-72, Cabot Corp., S_{BET} ~240 m² g⁻¹), graphite and aphanitic graphite oxide were prepared by a pulse-microwave assisted polyol route[22, 23]. Chloroplatinic acid with Pt content of 0.15 g was well mixed with ethylene glycol (EG, 100 mL) in a beaker by ultrasonic treatment for 30 min, and then 0.35 g carbon support (active carbon black, graphite or aphanitic graphite oxide) were added into the mixture. The pH value of the mixed suspension was adjusted to 10 by drop-wise addition of 1.0 mol L⁻¹ NaOH/EG solution. After dispersed with vigorous stirring and ultrasonication for 30 min, the Pt ions in the suspension were reduced to Pt⁰ by intermittent microwave-heating with pulses every 5 s for three times. After the reduction, the pH value of the suspension was adjusted to 2 using 0.01M HCl to promote the adsorption of the Pt nanoparticles onto the carbon support. The resulting electrocatalyst powders were filtered, washed and dried at 80 °C for 10 h in a vacuum oven. The as-prepared Pt electrocatalysts supported on active carbon black, graphite or aphanitic graphite oxide were denoted as Pt/CB, Pt/GC and Pt/MGO, respectively.

2.2 Structure characterization of supports and catalysts.

X-ray diffraction (XRD) patterns of the samples were recorded on a Rigaku D/MAX-RB diffractometer at 40 kV, 50mA, with a CuK α radiation and a counter rate of 2°/min from 2 θ =0.7° to 10°. For transmission electron microscopy (TEM) experiments, samples were first suspended in acetone (99.9 vol %) by ultrasonication, followed by deposition of the suspension on a lacey carbon grid. TEM images were obtained using an electron microscopy (JEOL JEM-2100F). The surface area was calculated by the Brunauer-Emmett-Teller (BET) method with Quantachrome Autosorb-1 analyzer at 77K. Before the measurements, samples were degassed for 12 h at 550 K.

2.3. Electrochemical measurement and fuel cell performance

Electrochemical measurements of the Pt electrocatalyst were performed on a galvanostat/potentiostat (Autolab, PGSTAT30) with a three-electrode cell at room temperature. A

saturated calomel electrode (SCE) and a platinum foil were used as the reference and counter electrodes, respectively. A glass carbon working electrode was polished using 0.3 and 0.05 μm alumina slurries, followed by washing with water and acetone. 1 mg of catalysts were dispersed ultrasonically in 1 mL Nafion solution (0.5 wt %) to obtain a homogeneous ink. A 10 μL of the ink was pipetted onto the working electrode surface. The coating was then dried at room temperature in air. The cyclic voltammograms were collected in a N_2 -saturated 0.5 M H_2SO_4 between -0.23 and 1.0 V with a scan rate of 10 mVs^{-1} . The working electrodes were electrochemically cleaned by continuous cycling at 50 mVs^{-1} until a stable response was obtained before the measurement curves were recorded.

3. RESULTS AND DISCUSSION

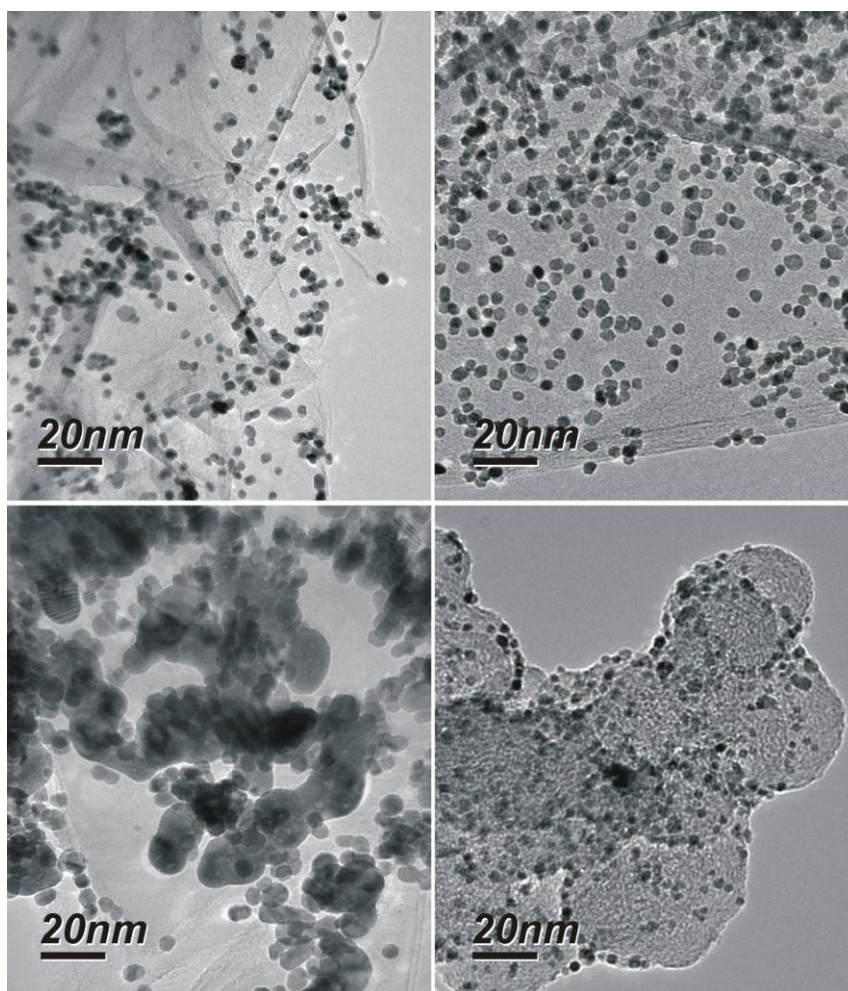


Figure 1. TEM images of Pt electrocatalysts supported on (a) microcrystalline graphite oxide at pH=11, (b) microcrystalline graphite oxide at pH=9, (c) flake graphite at pH=11, (d) carbon black at pH=11

Figure 1 presents the TEM images of Pt electrocatalysts supported on microcrystalline graphite oxide (a, b), graphite active (c) and carbon black (d). The average particle size of Pt/MGO displayed in

figure 1a is about 3.5 nm according to the measurement over 200 particles, very close to that of the Pt/CB catalyst (1d). However, in the case of inert graphite as the catalyst support, it is seen that the Pt nanoparticles easily form aggregates (1c). The reason for obtaining well dispersed and small sized Pt nanoparticles on the microcrystalline graphite oxide and carbon black supports could be understood by the enhanced noble metal anchoring through the activation of surface carbon atoms to functional groups such as carboxyl groups. The effect of carbon support functionalization on the dispersion of Pt nanoparticles was also demonstrated by the Figure 1b, which had Pt particles slightly large to about 3.8 nm when the pH value of the reaction solution was decreased to 9. In high pH value, the carboxyl groups on the carbon surface trends to expand with high zeta potential, and provided more active sites for Pt nanoparticles deposition.

To further understand the difference of the Pt dispersion on the various supports. The high-resolution C1s XPS spectra of Pt electrocatalysts support on microcrystalline graphite oxide, graphite and active carbon black were investigated and the results were displayed in Figure 2.

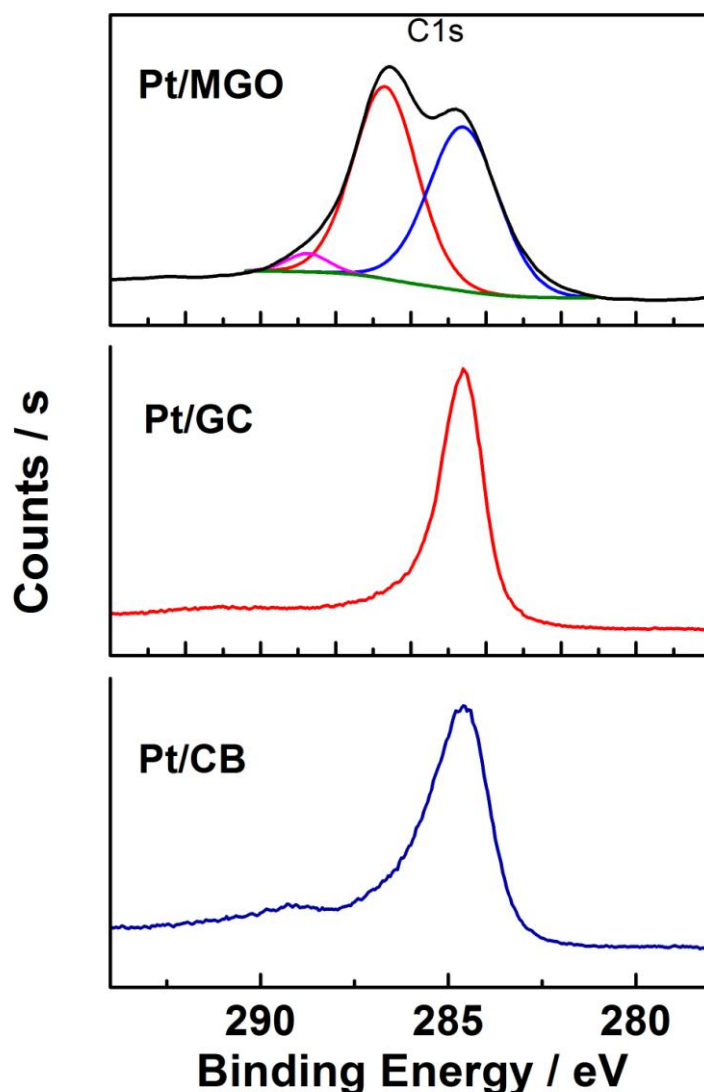


Figure 2. C1s XP spectral regions of (a) Pt/MGO, (b) Pt/GC and (c) Pt/CB

The fitting curves yield three components at ~ 284.9 , ~ 286.7 , and ~ 288.5 eV, corresponding to binding energies of carbon in C=C, C-O (hydroxyl and epoxy), and C=O (carboxyl and ketone) groups, respectively[24-27]. The relative peak intensities of the states are qualitatively similar to those previously reported using the Hummers synthetic protocol, showing that nearly 50% of carbon of microcrystalline graphite oxide is bonded to oxygen[28-30]. However, the spectrum shows small peaks in the region of C=C, suggested the maintaining of microcrystalline graphite structure which should be high resistant towards corrosion.

Further insight into the carbon-oxygen bonding is garnered from the O1s peak manifold, as displayed in Figure 3. A peak assigned to O=C is observed at 531.0 eV[31, 32], just as demonstrated in C1s curves. The peaks corresponding to those oxygen functional groups in the spectrum of graphite of Pt/GC were extensively low in comparison to that of Pt/MGO, demonstrating the low active sites for Pt deposition. Pt/CB has O=C at 531.0 eV and a second more intense component of HO-C at 532.4 eV (vide infra), which should be corresponding to the high dispersion of Pt particles on Pt/BC.

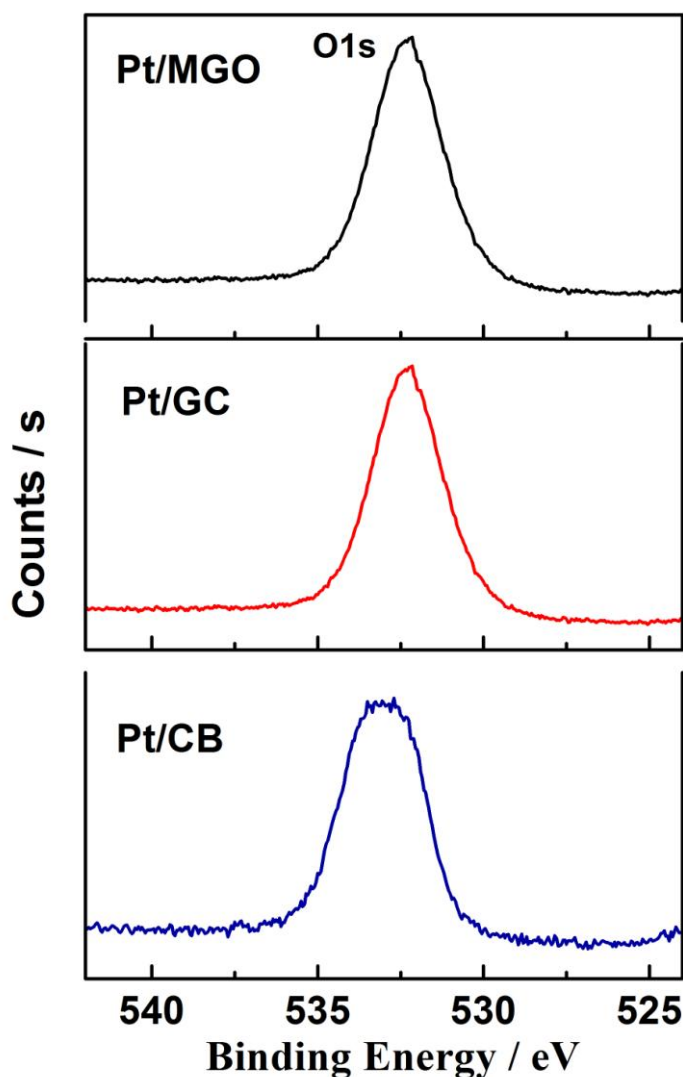


Figure 3. O1s XP spectral regions of (a) Pt/MGO, (b) Pt/GC and (c) Pt/CB catalyst

Figure 4 shows the XRD patterns of Pt electrocatalysts support on microcrystalline graphite oxide, graphite and active carbon black. For Pt/GC sample, the peaks at around 26° and 54° correspond to graphitic (002) and (004) reflection[33], respectively. For Pt/MGO, the intensity of graphitic (002) and (004) reflection are slightly reduced and an additional peak near 10° appeared which can be assigned to the (001) reflection of graphite oxide [34, 35]. The interlayer spacing of microcrystalline graphite oxide was calculated to be 0.9 nm, which is larger than that of graphite power (0.335 nm) due to the introduction of oxygen-containing functional groups on the graphite sheets. The XRD spectrum also present characteristic peaks of Pt nanoparticles at 39.8° and 46.5° , corresponding to platinum (111) and (200) reflection, respectively[36, 37]. Average Pt particle sizes calculated from the (111) diffraction signal widths of the samples are 3.86 nm, 5.65 nm and 2.75 nm for Pt/MGO, Pt/GC and Pt/CB, respectively. The calculated particles size of Pt/MGO and Pt/CB are good agreement with those from TEM data as shown in Figure. However, the calculated particles size of Pt/GC is smaller than that observed in TEM image. It is generally accepted that discrepancy of the sizes measured by XRD and TEM became greater as the particle sizes are bigger[38] due to the intrinsic difference between TEM and XRD, especially for the particles greater than ~ 5 nm. XRD is well known to be useful to measure average crystallite or domain sizes but not particle sizes whereas TEM measures individual particle sizes directly. As a result, if there are particles consisting of more than one crystallite, the particle sizes measured by XRD would be smaller than those obtained by TEM[39]. There is a higher probability of polycrystalline particles for the samples with bigger Pt sizes.

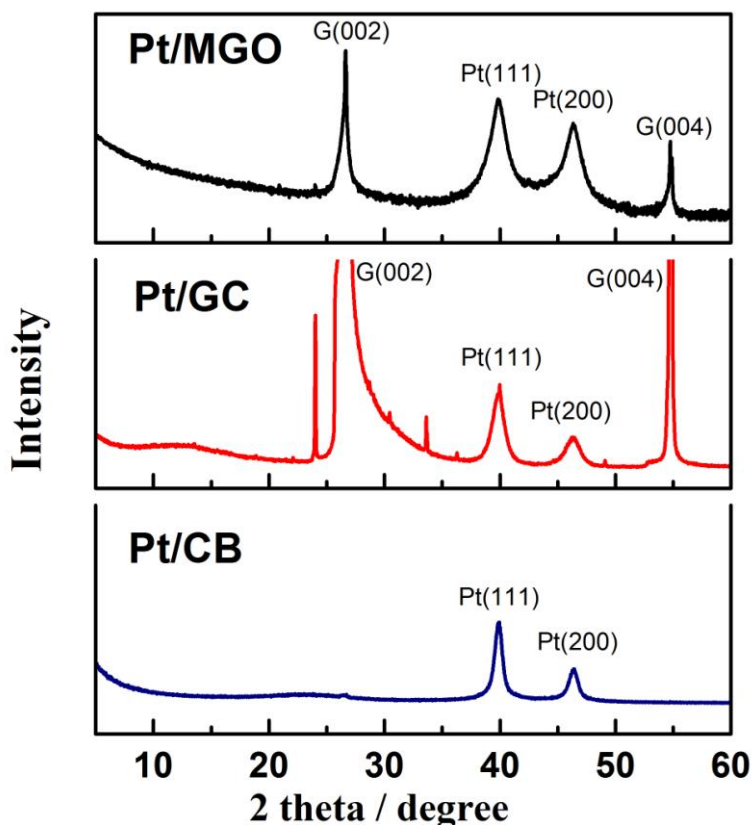


Figure 4. XRD patterns of (a) Pt/MGO, (b) Pt/GC and (c) Pt/CB catalyst

Figure 5 is the steady CVs of Pt/MGO, Pt/GC and Pt/CB catalyst at initial state and after 1000 CV circles. The results reveal clear hydrogen and oxygen evolution at the usual potentials for the initial CV. Excellent electrochemical activities of the Pt electrocatalyst can be observed from the CV curves. The electrochemically active surface (EAS) calculated from the hydrogen reaction charge for the Pt/MGO, the Pt/GC and the Pt/CB catalyst are $29.0 \text{ m}^2/\text{g}_{\text{Pt}}$, $5.1 \text{ m}^2/\text{g}_{\text{Pt}}$ and $11.7 \text{ m}^2/\text{g}_{\text{Pt}}$, respectively. In general, similar EAS of Pt/MGO electrocatalyst and Pt/CB is most likely due to the similar particle size of Pt nanoparticle on the two types of catalyst. The Pt/MGO catalyst has a slightly higher EAS than that of the Pt/CB suggests that some of the Pt particles interface attached to the carbon particles or dropped into the closed carbon capillaries. In this case, the adsorption and desorption of the H^+ on the catalyst surface is rather difficult than the Pt/MGO catalyst. As expected, the Pt/GC catalyst had the lowest initial ESA because of big Pt nanoparticles size. After 1000 CV circles, the Pt/CB catalyst showed a 23.08 % loss in catalytic surface area, while the Pt/GC exhibited an initial gain and finally a 19.61 % loss in catalytic surface area, suggesting the graphite could provide much higher durability than carbon black.

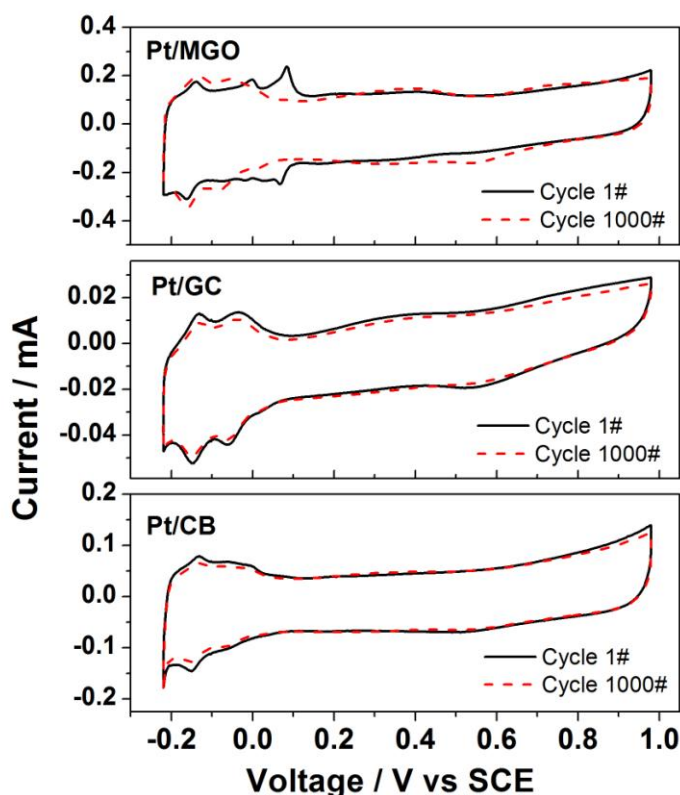


Figure 5. Cyclic voltammetric curves of (a) Pt/MGO, (b) Pt/GC and (c) Pt/CB electrocatalyst measured in a N_2 -saturated $0.5\text{M H}_2\text{SO}_4$ at a scan rate of 10 mV s^{-1} .

The Pt/MGO presents good balance between activity and durability in the CV accelerated test. After 1000 CV circles, the EAS loss of the Pt/MGO catalyst is 2.07 %, extensively lower than that of the Pt/CB catalyst and the Pt/GC catalyst. The high electrochemical stability of the Pt/MGO catalyst

should be contributed to the inherent inert MGO graphite structure. Another reason responded for the durability should be assigned for the close interaction between the MGO and Pt nanoparticles because of the functional groups. The functional groups act as anchoring centers for Pt nanoparticles, thus strengthening the interaction between the Pt nanoparticles and carbon support and improving the resistance of Pt nanoparticles to sintering during the test.

4. CONCLUSIONS

Microcrystalline graphite oxides have been prepared for developing highly durable Pt/C catalyst for fuel cells. Highly dispersed Pt nanoparticles with size about 3.5 nm were deposited on microcrystalline graphite oxide because of the highly functionalized surface. Cyclic voltammetric results demonstrated that the initial activity surface area of Pt/MGO catalyst was $29.0 \text{ m}^2/\text{g}_{\text{Pt}}$, much better than Pt/C catalyst with carbon black as the support ($11.7 \text{ m}^2/\text{g}_{\text{Pt}}$) because of the surface activity of microcrystalline graphite oxide. The Pt/MGO catalyst also presented durability much better than conventional Pt/C catalyst under acidic electrochemical conditions because of the innate stability of graphite structure. After 1000 CV circles, the EAS loss of the Pt/MGO catalyst was 2.07 %, extensively lower than that of the Pt/CB catalyst and the Pt/GC catalyst.

References

1. R. Lin, B. Li, Y. P. Hou, J. M. Ma. *Int. J. of Hydrogen Energy*, 34 (2009) 2369.
2. X. Z. Yuan, S. Zhang, H. Wang, J. Wu, J. C. Sun, R. Hiesgen, et al. *J Power Sources*, 195 (2010) 7594.
3. S. J. Ashton, M. Arenz. *Electrochem. Commun.*, 13 (2011) 1473.
4. J. Chen, J. B. Siegel, T. Matsuura, A. G. Stefanopoulou. *J. Electrochem. Soc.*, 158 (2011) B1164.
5. C. C. Hung, P. Y. Lim, J. R. Chen, H. C. Shih. *J. Power Sources*, 196 (2011) 140.
6. A. A. Kulikovskiy. *J. Electrochem. Soc.*, 158 (2011) B957.
7. S. Park, Y. Shao, H. Wan, V. V. Viswanathan, S. A. Towne, P. C. Rieke, et al. *J. Phys. Chem. C*, 115 (2011) 22633.
8. J. Zhang, C. Song, J. Zhang. *J. Fuel Cell Sci.Tech.*, 8 (2011) 051006-1.
9. L. C. Colmenares, A. Wurth, Z. Jusys, R. J. Behm. *J. Power Sources*, 190 (2009) 14.
10. Y. Ishigami, K. Takada, H. Yano, J. Inukai, M. Uchida, Y. Nagumo, et al. *J. Power Sources*, 196 (2011) 3003.
11. H. Schulenburg, B. Schwanitz, N. Linse, G. G. Scherer, A. Wokaun, J. Krbanjevic, et al. *J. Phys. Chem. C*, 115 (2011) 14236.
12. S. Takenaka, H. Matsumori, H. Matsune, M. Kishida. *Appl. Catal. a-Gen.*, 409 (2011) 248.
13. S. B. Yin, S. C. Mu, M. Pan, Z. Y. Fu. *J. of Power Sources*, 196 (2011) 7931.
14. W. M. Zhu, A. Ignaszak, C. J. Song, R. Baker, R. Hui, J. J. Zhang, et al. *Electrochim. Acta*, 61 (2012) 198.
15. S. V. Selvaganesh, G. Selvarani, P. Sridhar, S. Pitchumani, A. K. Shukla. *Fuel Cells*, 11 (2011) 372.
16. S. Pylypenko, K. Wood, A. Queen, R. O'Hayre, A. Dameron, T. Olson, et al. *Abstr. Am. Chem. Soc.*, 242 (2011) 264.

17. R. T. Lv, T. X. Cui, M. S. Jun, Q. Zhang, A. Y. Cao, D. S. Su, et al. *Adv. Funct. Mater.*, 21 (2011) 999.
18. H. S. Oh, H. Kim. *Adv. Funct. Mater.*, 21 (2011) 3954.
19. E. Yli-Rantala, A. Pasanen, P. Kauranen, V. Ruiz, M. Borghei, E. Kauppinen, et al. *Fuel Cells*, 11 (2011) 715.
20. G. M. Scheuermann, L. Rumi, P. Steurer, W. Bannwarth, R. Muelhaupt. *J. Am. Chem. Soc.*, 131 (2009) 8262.
21. P. Steurer, R. Wissert, R. Thomann, R. Muelhaupt. *Macromol. Rapid Commun.*, 30 (2009) 316.
22. H. Meng, P. K. Shen. *J. Phys. Chem. B*, 109 (2005) 22705.
23. H. Tang, S. P. Jiang. *J. Phys. Chem. C*, 112 (2008) 19748.
24. D. W. Lee, L. De Los Santos, J. W. Seo, L. L. Felix, A. Bustamante, J. M. Cole, et al. *J. Phys. Chem. B*, 114 (2010) 5723.
25. Z. Y. Lin, Y. G. Yao, Z. Li, Y. Liu, C. P. Wong. *J. Phys. Chem. C*, 114 (2010) 14819.
26. S. Park, J. An, J. R. Potts, A. Velamakanni, S. Murali, R. S. Ruoff. *Carbon*, 49 (2011) 3019.
27. Y. H. Zu, J. Y. Tang, W. C. Zhu, M. Zhang, G. Liu, Y. Liu, et al. *Bioresour. Technol.*, 102 (2011) 8939.
28. X. Li, G. Zhang, X. Bai, X. Sun, X. Wang, E. Wang, et al. *Nat. Nanotechnol.*, 3 (2008) 538.
29. D. Yang, A. Velamakanni, G. Bozoklu, S. Park, M. Stoller, R. D. Piner, et al. *Carbon*, 47 (2009) 145.
30. D. R. Dreyer, S. Park, C. W. Bielawski, R. S. Ruoff. *Chem. Soc. Rev.*, 39 (2010) 228.
31. M. Seredych, A. V. Tamashausky, T. J. Bandosz. *Adv. Funct. Mater.*, 20 (2010) 1670.
32. C. D. Zangmeister. *Chem. Mater.*, 22 (2010) 5625.
33. J. Bian, M. Xiao, S. J. Wang, Y. X. Lu, Y. Z. Meng. *Catal. Commun.*, 10 (2009) 1529.
34. T. A. Pham, N. A. Kumar, Y. T. Jeong. *Synth. Met.* 160 (2010) 2028.
35. J. Wu, S. Bai, X. Shen, L. Jiang. *Appl. Surf. Sci.*, 257 (2010) 747.
36. T. Hyde. *Platinum Met. Rev.*, 52 (2008) 129.
37. M. Pan, H. L. Tang, S. C. Mu, R. Z. Yuan. *J. Mater. Res.*, 19 (2004) 2279.
38. Z. L. Liu, B. Guo, L. Hong, T. H. Lim. *Electrochem. Commun.*, 8 (2006) 83.
39. K. S. Han, Y. S. Moon, O. H. Han, K. J. Hwang, I. Kim, H. Kim. *Electrochem. Commun.*, 9 (2007) 317